

Real-time evolution of a laser-dressed Helium atom: Attosecond-resolved two-color photoionization study

Niranjan Shivaram,¹ Henry Timmers,¹ Xiao-Min Tong,² and Arvinder Sandhu^{1,*}

¹*Department of Physics, University of Arizona, Tucson, AZ, 85721 USA.*

²*Center for Computational Sciences, University of Tsukuba, Ibaraki 305-8573, Japan.*

(Dated: June 18, 2022)

Using extreme-ultraviolet attosecond-pulse-trains, we investigate the photoionization dynamics of a Helium atom in the presence of moderately-strong ($\sim 10^{12} \text{Wcm}^{-2}$) femtosecond laser pulses. The electronic structure of a laser-dressed atom is traced in real-time through precision measurements of ion-yields and photo-electron angular distributions. Quantum interferences between photo-excitation paths are interpreted using the Floquet formalism. As the laser pulse intensity ramps on femtosecond timescales, we observe transitions between ionization channels mediated by different atomic resonances. The quantum phase of interfering paths is extracted for each channel and compared with simulations. Our results elucidate photoionization mechanisms in strong-fields and open the doors for photo-absorption/ionization control schemes.

The recent advances in ‘attosecond science’ have given a new impetus to the study of atomic and molecular phenomena by providing direct real-time access to electron dynamics[1]. Experiments in this regime are typically conducted using extreme-ultraviolet (XUV) attosecond pulses or pulse trains along with precisely synchronized strong-field femtosecond near-infrared (IR) laser pulses, to obtain new insights into dynamics of electronically excited systems[1–3]. As the roots of ‘attosecond science’ lie in the strong-field concepts developed in 1990’s [4], the application of new attosecond techniques to refine our understanding of atomic/molecular dynamics in strong fields is of particular interest[1].

Here, we report precision real-time measurements of the transient non-equilibrium electronic structure of Helium in intense fields. We investigate the quantum interferences in two-color photo-ionization pathways using XUV attosecond pulse trains (APT) and variable strength near-infrared (IR) laser fields. As the field intensity changes on femtosecond timescales, we observe switching between ionization channels. We find that yield from each resonance-mediated ionization channel oscillates with a specific phase. We interpret this quantum phase using Floquet interaction model. Numerical calculations using time-dependent Schrödinger equation (TDSE) serve to elucidate the important role of Floquet interferences in photo-excitation and ionization.

We use amplified 65fs, 785nm IR pulses of 1.5mJ energy, which are split into two parts. One part is focused onto a Xe gas-filled hollow waveguide to generate APT of high-harmonics(HH). The APT along with the co-propagating driving infrared pulse (IR_d) is focused onto a He gas jet using a toroidal mirror. The second part, a probe pulse (IR_p), goes to a delay stage and is focused on the He target with a 50cm lens. The schematic of our experimental set-up is provided in [5]. Photo-electrons are imaged using a velocity-map-imaging (VMI) setup. He^+ ions are spatially imaged such that there is a one-to-one correspondence between the point of origin and

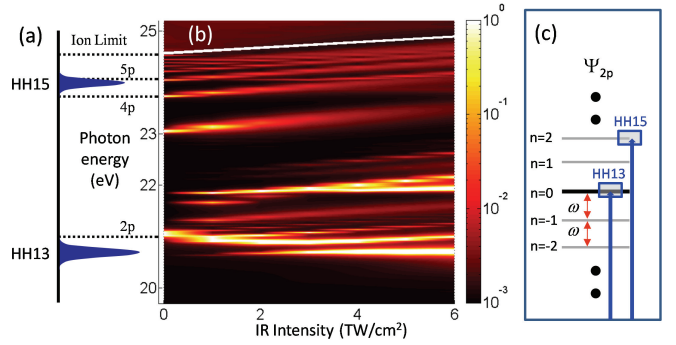


FIG. 1. (a) XUV spectrum and the relevant He states (b) Calculated XUV photoabsorption cross-section as a function of laser intensity. (c) Floquet manifold showing one-photon spaced components of IR-dressed 2p state and the two interfering paths associated with HH13 and HH15 excitation.

the point they hit the detector, allowing us to eliminate Gouy phase averaging and obtain a high-quality signal[5].

Fig. 1(a) schematically shows the experimental HH spectra relative the unperturbed He resonances. The 15th harmonic is resonant with the 5p electronic state and 13th harmonic is slightly below 2p resonance. Two other harmonics that we observe, i.e. 11th and 17th, are much weaker (20 times lower) and non-resonant, hence they do not play a significant role in this study. In Fig. 1(b) we show the photo-absorption cross-section of He as a function of photon energy and peak IR intensity calculated using the method described in [6]. Clearly, the discrete atomic resonances evolve into a complicated structure even in a moderately intense laser field of the order of 10^{12}Wcm^{-2} . The higher excited-states (3p, 4p, 5p, etc.) exhibit positive shifts, which can be approximated by the ponderomotive effect. The low-lying 2p state exhibits a negative shift and develops multiple branches. At intensities around $5 \times 10^{12} \text{Wcm}^{-2}$, the excited state structure bears very little resemblance to the unperturbed case.

In previous experiments with APT and IR, it has been observed that the He^+ ion yield oscillates as a function of time delay with half-IR-cycle periodicity [7–9]. This has been interpreted as interference between wave packets generated by successive bursts in the APT[7, 10, 11]. Using Floquet interaction picture[12], it has been shown that the interference between different Fourier components of an IR dressed state leads to this oscillatory variation of ionization probability at 2ω frequency[9, 13]. Importantly, recent theoretical work[13] has raised crucial questions about the role of different ionization paths and the phase of ionization signal that have not been addressed by the experimental studies conducted so far. Here we measure the *phase* of the ion-yield oscillations and investigate its variation in terms of the evolution of laser-dressed atomic structure. We demonstrate that for a given IR-dressed atomic resonance (Fig. 1(c)), the quantum phase difference between the dipole transitions to different Fourier components determines the oscillation phase of the ionization signal.

In our XUV+IR ionization measurements, the IR field results from a combination of two IR pulses. The weaker pulse (IR_d) is phase-locked to the APT and the stronger pulse (IR_p) is time delayed relative to the APT[5]. For two main harmonics (HH13 and HH15 in our case), the probability of ionization by the XUV and combined IR field can be obtained for a given Floquet state as [13]

$$P(\tau) \propto \left| M_0 f_0 + M_2 f_2 e^{-i(2\omega\tau + 2\delta_0 - 2\delta(\tau) + \phi)} \right|^2 \quad (1)$$

where $M_0(A(\tau))$ and $M_2(A(\tau))$ are the IR-intensity dependent matrix elements representing transitions to the direct and two-photon-dressed Fourier component. The terms f_0 and f_2 are the strengths of two harmonics, ω is the central frequency of the IR, τ is the time delay between XUV and probe IR, δ_0 is the phase at which the attosecond pulse is locked to the driver IR field. The quantum phase difference between M_0 and M_2 , which is an important quantity in the paper, is represented by ϕ . Figure 1(c) diagrammatically shows the Floquet manifold associated with 2p resonance and the two interfering excitation paths discussed above.

The delay dependence of combined IR amplitude and phase, i.e. $A(\tau)$ and $\delta(\tau)$, is given as $A(\tau) = (A_p^2 + A_d^2 + 2A_p A_d \cos(\omega\tau))^{1/2}$ and $\delta(\tau) = \sin^{-1}(A_d \sin(\omega\tau)/A(\tau))$, where A_p and A_d are the amplitudes of the probe and driver IR fields. For a weak driver-IR field ($A_d \ll A_p$), the dominant frequencies in $P(\tau)$ are 1ω and 2ω . We define the normalized amplitude of ion-yield oscillation as $P_{osc}(\tau) = (P(\tau) - P_{avg})/P_{avg}$, where P_{avg} is the one-cycle average. The P_{osc} in the weak driver case can then be approximated as

$$P_{osc}(\tau) = T_1 \cos(\omega\tau) + T_2 \cos(2\omega\tau + 2\delta_0 + \phi) \quad (2)$$

where T_1, T_2 are the amplitude factors.

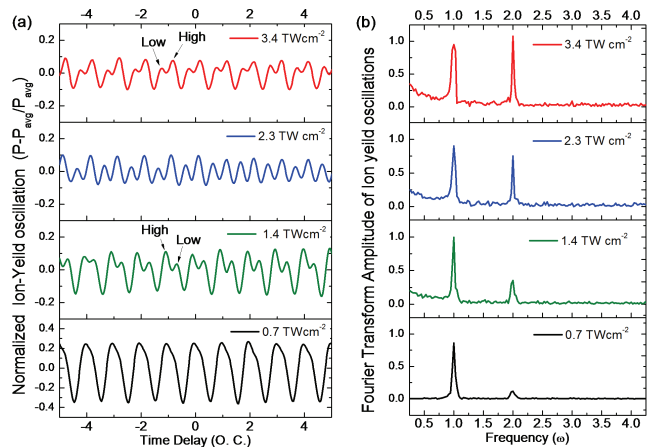


FIG. 2. (a) Normalized He^+ ion-yield oscillations for XUV and 2IR pulses (driver and probe) at different probe peak intensities (o.c. denotes optical cycles). Asymmetry in the double peak oscillation structure is reversed between 1.4 TWcm^{-2} and 3.4 TWcm^{-2} . (b) Fourier amplitude of ion-yield oscillations shows two prominent frequencies.

Figure 2(a) shows normalized experimental He^+ ion-yield as a function of the time delay between APT+ IR_d and probe IR_p at different probe IR intensities. The driver IR intensity is less than 10^{10}Wcm^{-2} . We observe a distinct oscillation structure with one-cycle and half-cycle components in accordance with equation (2). The oscillation at 1ω frequency, which arises from the intensity modulation due to the IR-IR interference, acts as a reference with respect to which we can robustly measure the phase ϕ of the Floquet path interferences occurring at 2ω . The 2IR method thus allows use to compensate for the interferometric drifts and other experimental variations. Furthermore, this approach also provides a method to measure δ_0 , which represents the timing of attosecond bursts relative to the peak of driving IR field.

Fig. 2(b) shows the Fourier transform of ion-yield oscillations over the time-delay range that spans more than 20 optical cycles. At low intensities, the 1ω component dominates, however, as the probe intensity is increased, the 2ω component increases. This is expected as the IR amplitude modulation decreases and the two-photon dressed Floquet contribution (i.e. M_2 in equation (1)) becomes increasingly important with intensity, leading to a stronger interference signal. Importantly, the oscillatory structure in Fig. 2(a) at two probe intensities, namely, 1.4 TW cm^{-2} and 3.4 TW cm^{-2} is very different. The asymmetric double-peak structure at 1.4 TW cm^{-2} shows the left-peak to be higher, whereas, at 3.4 TW cm^{-2} the situation is reversed and the right-peak is higher. This difference in oscillation structure is a direct manifestation of the change in phase relationship between the 2ω and 1ω components. The intensity dependent change in relative phase originates from the change

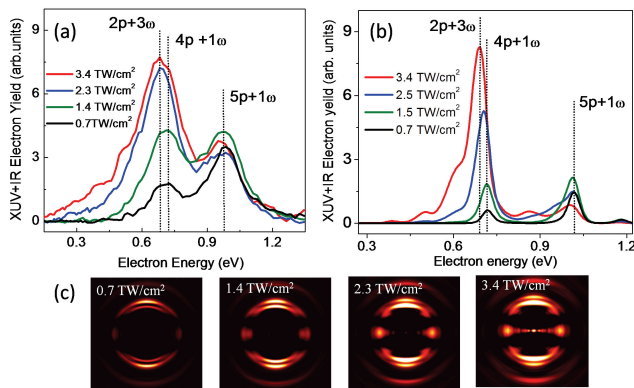


FIG. 3. (a) Experimental XUV+IR photo-electron spectrum of He at different IR probe intensities. As the IR intensity is increased the $2p + 3\omega$ peak becomes dominant. (b) Calculated photo-electron spectrum (c) Experimental VMI of photo-electrons at different IR probe intensities.

in value of ϕ in eq.(1), which represents the phase difference between the two interfering contributions. Before we quantitatively discuss this phase, it is important to identify the Floquet states contributing to the ionization.

To identify the Floquet paths, we utilize photoelectron spectroscopy. Fig. 3(a) shows the experimental electron spectra at probe intensities used in Fig. 2. The observed electron peaks in Fig. 3(a) are associated with IR ionization of XUV excited $5p$, $4p$ and $2p$ atomic states. At low intensities, the ionization is mediated by $5p$ resonance, and we observe a strong peak corresponding to $5p + 1\omega$ process. This is expected as 15th harmonic is initially resonant with $5p$ state. As the intensity is increased, the $4p + 1\omega$ starts contributing. At higher intensities the $2p + 3\omega$ channel dominates the ionization signal. This observation is in accord with Fig. 1(b) as the $2p$ structure Stark shifts downward in energy with increasing intensity, becoming resonant at higher intensities.

TDSE calculations for comparable intensity parameters also yield similar results (Fig. 3(b)). The angle-resolved photoelectron images in Fig. 3(c) also show that as intensity is increased towards 3.4 TWcm^{-2} , side lobes corresponding to the ‘g-wave’ structure appear. This another indication of 3-photon ionization of XUV excited state $2p$ state. Thus, the results from Fig. 3 confirm that the dominant two-color ionization pathway changes from the $5p$ -mediated ionization at low intensities to $2p$ -mediated ionization signal at higher intensities. Next, we extract the phases for various resonance mediated ionization channels and establish quantitative relationship between the strong-field variation of atomic structure and intensity dependent phase change observed in ion-yield oscillations of figure 2.

Figs. 2 and 3 show that even moderately intense laser pulses can significantly modify an atom and its ionization dynamics. Now we probe these transient dynamics

in real time. Fig. 4(a) shows the raw He^+ ion yield as a function of time-delay at 3.4 TW cm^{-2} probe intensity. The negative time-delay axis implies that the IR probe arrives ahead of the XUV pulse. As the time-delay changes from -20 o.c. towards zero, the asymmetric 2ω oscillation structure develops and evolves from high-left-peak asymmetry to high-right-peak asymmetry. Note that this behavior is similar to Fig. 2, except that Fig. 2 shows the dependence of ionization signal on peak intensity, whereas, Fig. 4(a) explores the dependence on intensity variation within the IR pulse profile.

Next, we extract the phase of 2ω component of ion-yield oscillations relative to the 1ω component using standard Fourier-transform methods. Figure 4(b) plots this phase as a function of the time-delay (solid line). We repeat the phase extraction exercise on the ionization signals in Fig. 2(a) and obtain the phase of 2ω component at different peak intensities. Assuming a Gaussian profile, we calibrate the time-delay axis such that each delay value corresponds to a specific instantaneous intensity (top-axis of Fig. 4(b)). Thus, we can plot the phases extracted from Fig. 2(a) as square dots in Fig. 4(b) and compare them with delay-dependent phase curve. A good match between the two independent results demonstrates the soundness of our experimental method.

The insets in figure 4(b) show the TDSE results for XUV+IR ionization oscillation at 3.4 TWcm^{-2} and 1.5 TWcm^{-2} with arrows pointing to comparable experimental points. At 3.4 TW cm^{-2} , where $2p$ contribution strongly dominates, the phase of 2ω oscillations is zero (right-inset), implying ionization yield maximizes when APT arrives at the peak of IR-field. We can use this fact to extract the δ_0 in eq. (2) and remove APT timing offset from our phase deduction, thereby setting the starting point of experimental phase value to zero. With this adjustment, the modified form of eq. (1) becomes

$$P(\tau) \propto \left| M_0 f_0 + M_2 f_2 e^{-i(2\omega\tau + \phi)} \right|^2 \quad (3)$$

Starting from zero, as we move to longer time-delays (i.e. lower intensities), the experimental phase value increases. The phase goes through π and reaches 1.5π at 1.4 TWcm^{-2} intensity. The TDSE calculation (left-inset) also yields a similar result as the 2ω oscillations in shifted in phase by $\sim 1.5\pi$ at 1.5 TWcm^{-2} .

The variation of phase figure 4(b) can now be understood in terms of the quantum mechanical phases associated with various ionization channels and the relative dominance of different channels. The calculated energy-resolved photoelectron data in figure 4(c) elucidates the role of different channels. At high intensity (3.4 TW cm^{-2}), the $2p$ resonance mediated ionization channel at 0.69 eV dominates. The oscillation of this channel has zero phase and the ionization yield peaks at zero-delay where XUV pulses arrive at the peak of IR field. For this to happen the quantum phase ϕ between the M_0 and M_2

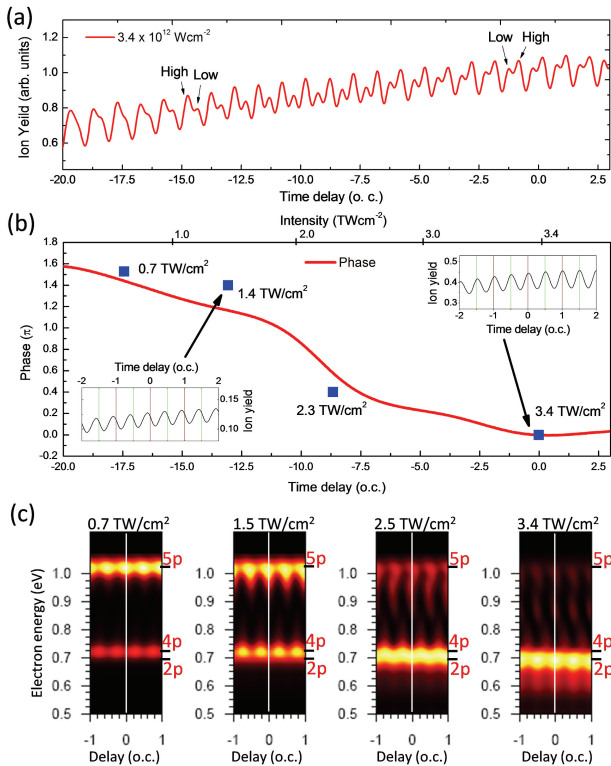


FIG. 4. He^+ ion yield as a function of time-delay at 3.4 TWcm^{-2} probe intensity. (b) The phase of the 2ω component of ion-yield oscillations with time delay. (c) TDSE results showing the energy-resolved oscillations in electron yield of various resonance mediated ionization channels.

transition matrix elements in eq. (3) has to be zero. In other words, 13HH and 15HH induced transitions to the Floquet components associated with 2p excitation are ‘in-phase’ (Fig. 1(c)).

As intensity decreases, the 4p channel at 0.72 eV starts contributing substantially. Interestingly, the oscillations in this channel are completely out of phase with the 2p contribution (Fig. 4(c), 1.5 TW cm^{-2}). Using eq. (3), this implies that $\phi = \pi$ for 4p mediated ionization channel and the ionization yield peaks at the zeros of the IR field. In Floquet picture, the 13th and 15th HH transition matrix elements to the components of 4p Floquet state have opposite signs. In general, as the transition matrix elements are real, ideally there are only two possibilities; either M_0 and M_2 can have the same sign ($\phi = 0, \pm 2\pi, \dots$) or opposite signs ($\phi = \pm\pi, \pm 3\pi, \dots$) and we see both varieties in Fig. 4(c). At very low intensity, the 5p ionization starts dominating and oscillates with same phase as 2p (i.e. $0, \pm 2\pi$). Thus, in our experiment, as the intensity decreases or time-delay get longer, we observe a change in phase of ion-yield oscillation, going from zero when 2p is dominant, through π where 4p contributes substantially, and eventually towards 2π where 5p dominates.

Our work represents a direct measurement of quan-

tum phases associated with XUV+IR ionization channels, which are not known *a priori*. These observations are general and should be valid whenever XUV excitation occurs in a strong field. As the modification of electronic states depends on the instantaneous value of the IR laser intensity at the time of XUV excitation, tuning IR intensity can change contribution of the different matrix elements to the interfering terms. By precisely controlling the XUV spectrum, IR intensity and the time-delay between the APT and IR, it is possible to control the ionization dynamics. A recent experiment[14] demonstrating XUV transparency validates some of these ideas.

In conclusion, the two-color photo-ionization of He by XUV and IR pulses represents a relatively simple yet rich system for exploration of light-matter interaction. We show that even a moderately strong field, often used in XUV-IR pump-probe studies, can substantially modify electronic structure and ionization dynamics on attosecond timescales. We identify different ionization channels and measure the quantum phases associated with these Floquet paths, which is the first such measurement to our knowledge. Understanding the evolution of atomic structure in strong fields and its interaction with attosecond XUV pulses can provide us with a knob for fine control of photo-dynamics.

This work was supported by the National Science Foundation (NSF) under contract PHY-0955274.

* sandhu@physics.arizona.edu

- [1] F. Krausz and M. Ivanov, Rev. Mod. Phys. **81**, 163 (2009).
- [2] A. S. Sandhu, E. Gagnon, R. Santra, V. Sharma, W. Li, P. Ho, P. Ranitovic, C. L. Cocke, M. M. Murnane, and H. C. Kapteyn, Science **322**, 1081 (2008).
- [3] H. Wang, M. Chini, S. Y. Chen, C. H. Zhang, F. He, Y. Cheng, Y. Wu, U. Thumm, and Z. H. Chang, Physical Review Letters **105**, 143002 (2010).
- [4] P. B. Corkum, Phys. Rev. Lett. **71**, 1994 (1993).
- [5] N. Shivaram, A. Roberts, L. Xu, and A. Sandhu, Optics Letters **35**, 3312 (2010).
- [6] X. M. Tong and N. Tushima, Physical Review A **81**, 063403 (2010).
- [7] P. Johnsson, J. Mauritsson, T. Remetter, A. L’Huillier, and K. J. Schafer, Phys. Rev. Lett. **99**, 233001 (2007).
- [8] P. Ranitovic *et al.*, New J. Phys. **12**, 013008 (2010).
- [9] X. M. Tong, P. Ranitovic, C. L. Cocke, and N. Tushima, Physical Review A **81**, 021404 (2010).
- [10] P. Riviere, O. Uhden, U. Saalmann, and J. M. Rost, New Journal of Physics **11**, 053011 (2009).
- [11] M. Holler, F. Schapper, L. Gallmann, and U. Keller, Physical Review Letters **106**, 123601 (2011).
- [12] S. I. Chu and D. A. Telnov, Phys. Rep. **390**, 1 (2004).
- [13] X. M. Tong and N. Tushima, Phys. Rev. A **81**, 043429 (2010).
- [14] P. Ranitovic, X. M. Tong, C. W. Hogle, X. Zhou, Y. Liu, N. Tushima, M. M. Murnane, and H. C. Kapteyn, Physical Review Letters **106**, 193008 (2011).